Ligand Displacement Exposes Binding Site Heterogeneity on CdSe Nanocrystal Surfaces

Emile Drijvers,[†,‡] Jonathan De Roo,[†,¶] José C. Martins,[§] Ivan Infante,[‖] and Zeger Hens[*,†,‡]

Department of Inorganic and Physical Chemistry, Ghent University, Belgium, Center for Nano and Biophotonics, Ghent University, Ghent, Belgium, Department of Chemistry, Columbia University, New York, USA, Department of Organic and Macromolecular Chemistry, Ghent University, Belgium, and Department of Theoretical Chemistry, Vrije Universiteit Amsterdam, Amsterdam, The Netherlands

E-mail: zeger.hens@ugent.be

Nanocrystal-ligand interactions and ligand exchange processes are usually described by a uniform distribution of equal binding sites. Here, we analyze this assumption by a quantitative study of the displacement of Z-type cadmium oleate ligands from CdSe nanocrystals by addition of L-type ligands. First, we determined the stoichiometry of the displacement reaction by analyzing the equilibrium upon dilution using solution nuclear magnetic resonance spectroscopy. We found that 1 equivalent of tetramethylethylene-1,2-diamine (TMEDA) or two equivalents of n-butylamine or benzylamine bind the displaced cadmium oleate. We only reached a comprehensive description of the displacement isotherm by including two types of

[*]To whom correspondence should be addressed
[†]Department of Inorganic and Physical Chemistry, Ghent University, Belgium
[‡]Center for Nano and Biophotonics, Ghent University, Ghent, Belgium
[¶]Department of Chemistry, Columbia University, New York, USA
[§]Department of Organic and Macromolecular Chemistry, Ghent University, Belgium
[‖]Department of Theoretical Chemistry, Vrije Universiteit Amsterdam, Amsterdam, The Netherlands

binding sites with a different equilibrium constant. We corroborated this finding by density functional theory calculations on a CdSe model nanocrystal, which show that even single facets contain a broad variety of binding sites. Finally, we analyzed the thermodynamics of the displacement equilibrium for the weaker binding sites by constructing van 't Hoff plots for the different displacers. Whereas displacement with TMEDA appears to be enthalpically neutral, it is entropically favorable. In contrast, displacement with the primary amines is entropically unfavorable but is associated with a negative change in enthalpy. Since the distribution of binding energy emanates from the large fraction of edge and vertex sites on a nanocrystal facet, these findings are most likely inherent to nanocrystals in general and should be considered when analyzing surface reactions on such materials.

Introduction

The way organic or inorganic moieties terminate nanocrystal surfaces plays a key role in the emerging research field of colloidal nanocrystals (NCs).[1,2] The specific binding of organic ligands to nanocrystal surfaces is used to control the size and shape of NCs as they grow in a reaction mixture.[3–6] Moreover, the resulting ligand capping stabilizes NC dispersions by steric hindrance and facilitates the homogeneous dispersion of NCs in solvents or polymer matrices.[7,8] In addition, ligands play a role in the physical properties of NCs.[9–12] In the case of semiconductor NCs or quantum dots (QDs), they can suppress non-radiative recombination of electron-hole pairs by passivating electronic trap states at the nanocrystal surface or they can be used to adjust the QD work function.[10,13,14] Both aspects are decisive for using QDs in lighting and display applications, or photovoltaics and photodetection, respectively.[15–17] As a result, the formation of nanocrystals with a well-controlled, predefined surface composition, for example in terms of ligand type and the ligand surface concentration, has become a central element in nanocrystal science and technology.[18–23]

The recent focus on binding motifs greatly enhanced insight in nanocrystal-ligand binding by using the covalent bond classification,[24] developed for metal-ligand complexes, to describe the binding of ligands to nanocrystals.[2,13] Here, ligands were labeled L, X or Z depending on the number of electrons they provide to the nanocrystal-ligand bond (2, 1 or none, respectively), and a number of generic binding motifs were identified.[2] In the case of metal chalcogenide nanocrystals, such as CdSe, CdTe, PbS and PbSe, the prevailing motif involved the binding of X-type ligands, with examples including carboxylates, phosphonates and thiolates, to a nanocrystal surface enriched in metal cations.[1,13,25–29] This class will be indicated henceforth as [ME](MX_2), where M is a divalent metal such as Cd or Pb, and E stands for S, Se or Te. The adaptation of this classification to describe NC surface chemistry led to the development of controlled ligand displacement reactions. Here, a notable example is the so-called L-type driven Z-type displacement, a reaction in which L-type ligands are used to displace entire MX_2 units from the surface of an ME nanocrystal by formation of an $L-MX_2$ complex (see Figure 1).[13] This displacement reaction enables the Z-type ligand concentration to be precisely controlled, a property that has been used to establish the relation between ligand surface concentration and photoluminescence quantum yield,[13] to promote nanocrystal epitaxy,[30] or to extract organic ligands from nanocrystal films.[31–33] Such examples attest to the need for a better understanding of L-type driven Z-type displacement. At best, this involves reaction equations and equilibrium constants, by which the degree of ligand displacement can be predicted upfront. Furthermore, recent surface chemistry studies

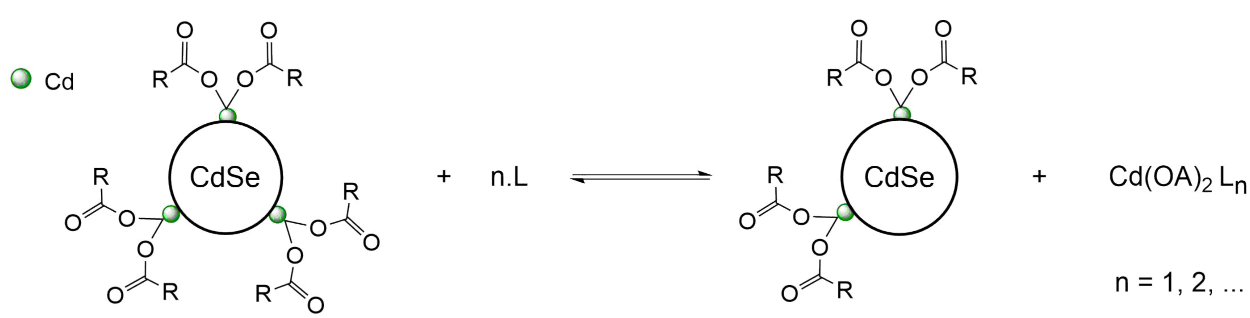

Figure 1: Cartoon representation of the L-type promoted Z-type displacement reaction on a CdSe NC surface. The initial Z-type $CdOA_2$ ligand can be displaced then complexed by one or more L-type ligands.

are depicting NCs where the capping ligands are demonstrated to possess different binding energies relating to different binding sites or facets,[34,35] and more studies are still required to fully understand and control the surface chemistry of NCs.

Here, we study the stoichiometry of the displacement of cadmium oleate from CdSe nanocrystals and the thermodynamics of its isotherm using solution nuclear magnetic resonance (NMR) spectroscopy. Through dilution experiments, we demonstrate that 1 equivalent of TMEDA displaces 1 equivalent of cadmium oleate, whereas the displacement reaction needs 2 equivalents of benzylamine or butylamine. In each case, the displacement isotherm is well described by a two-site model that involves the binding of cadmium oleate to two different surface sites with distinct equilibrium constants. We estimated the thermodynamic descriptors of the weaker binding sites by van 't Hoff analysis. We further underscore the validity of a multiple-site model by means of DFT calculations, which indeed yield a distribution of binding sites, even on a single crystal facet. This variety of binding sites is linked to the presence of facet edges and vertices, and the possibility or not of surface reconstruction after ligand displacement. Importantly, the DFT calculations and the experimental results yield comparable fractions of weaker binding sites and comparable displacement energies, indicating that these are effectively the ligands displaced at low displacer concentrations. Given the propensity of ligands to bind to the sites with the highest binding energy, surface reactions will thus face a subpopulation of ligands that can be very difficult to strip or exchange. In addition, the fraction of weakly bound ligands will strongly depend on the initial ligand density, and thus the sample history and cleaning procedure. Moreover, since the distribution of binding energies is contingent on the presence of edge and vertex sites, and site-dependent surface reconstructions, binding site heterogeneity is most likely inherent to the nature of nanoscale crystals. As such these results are most likely not limited to CdSe NCs.

Experimental Section

Materials. CdO (99.99%) and 1,2-dichlorobenzene-d_4 (DCB, 98% deuterated) were purchased from Sigma-Aldrich. Selenium powder (Se, -200 mesh, 99.999%), oleic acid (OA, 90%) and 1-octadecene (ODE, 90%) were purchased from Alfa Aesar. Toluene, isopropanol and methanol were purchased from Fiers.

Synthesis and Characterization of Zinc Blende CdSe NCs. The CdSe NCs were synthesized using a heterogeneous ODE-Se precursor mixture and under atmospheric conditions as described by Flamee *et al.*[36] Here, 0.642 g (5 mmol) of CdO, 4.236 g (15 mmol) of oleic acid and 25 mL of 1-octadecene were mixed in a 50 mL three-neck flask. The mixture was heated to 270℃ and 2.25 mL of a 2 M heterogeneous ODE-Se mixture (4.5 mmol) was swiftly added to the reaction mixture. The reaction was quenched with a water bath after 2 minutes. Once the reaction mixture was at room temperature, 20 mL of isopropanol, 20 mL toluene and 20 mL MeOH were added. The mixture was the centrifuged at 4000 rpm for 5 min and the supernatant was discarded. The NCs were purified three more times using minimum amounts of toluene and methanol. The resulting NCs were redispersed and stored in 3 mL toluene. The size of the CdSe NCs was determined from the position of the first excitonic absorption peak using this zb-CdSe sizing curve.[37] The concentration of the NC dispersion was determined based on their absorption at 300, 320 and 340 nm and their intrinsic absorption coefficient at these respective wavelengths.[37]

NMR Experiments. The NMR samples were prepared by drying the CdSe NCs under a nitrogen flow which were then redispersed in 500 μL of 1,2-dichlorobenzene-d_4. The NMR data were collected on a Bruker Avance II spectrometer operating at a ^{1}H frequency of 500.13 MHz and equipped with a PATXO probe (^{1}H, ^{13}C and ^{19}F). The temperature of the measured sample was tuned from 298.15 K to 403.15 K depending on the experiment type. Quantitative ^{1}H spectra were realized by using the Digital ERETIC method with a 20 s delay between scans to allow for full relaxation.

Density Functional Theory Calculations. All calculations were performed at the DFT level[38] with a PBE exchange-correlation functional.[39] Core electrons were included using an effective core-potentials, while valence electrons were described with a double-zeta basis-set augmented with polarization functions (DZVP).[40] Calculations have been carried out using the CP2k 3.0 code.[41] Further details on the nanocrystal model are provided in the main text.

Results and Discussion

Ligand Displacement as Observed by NMR Spectroscopy

We synthesized zinc blende CdSe NCs (see Supporting Information, Section S1) according to the protocol developed by Flamee *et al.*[36] Figure 2a represents the solution ^{1}H NMR spectrum of a purified dispersion of 3.4 nm CdSe NCs in 1,2-dichlorobenzene-d_4, together with the spectrum of oleic acid in the same solvent. The CdSe NC spectrum features the broadened resonances that are characteristic of bound oleate – denoted as the [CdSe]($CdOA_2$) spectrum henceforth – which were assigned according to previous literature reports as indicated in Figure 2a.[26]

Upon addition of butylamine ($BuNH_2$), an L-type ligand expected to displace cadmium oleate from the CdSe surface, the [CdSe]($CdOA_2$) NMR spectrum shows some notable changes. Next to the characteristic resonances of $BuNH_2$ appearing at 2.6 ppm in 1,2-dichlorobenzene-d_4, one sees that all the originally bound oleate resonances lose intensity and acquire a second resonance at lower chemical shift. This observation is exemplified in more detail for the alkene resonance **5** and the $\alpha - CH_2$ resonance **1** in Figure 2b. The latter is probably the most striking example since the $\alpha - CH_2$ resonance of bound oleate can hardly be observed in the [CdSe]($CdOA_2$) spectrum due to excessive broadening, whereas it

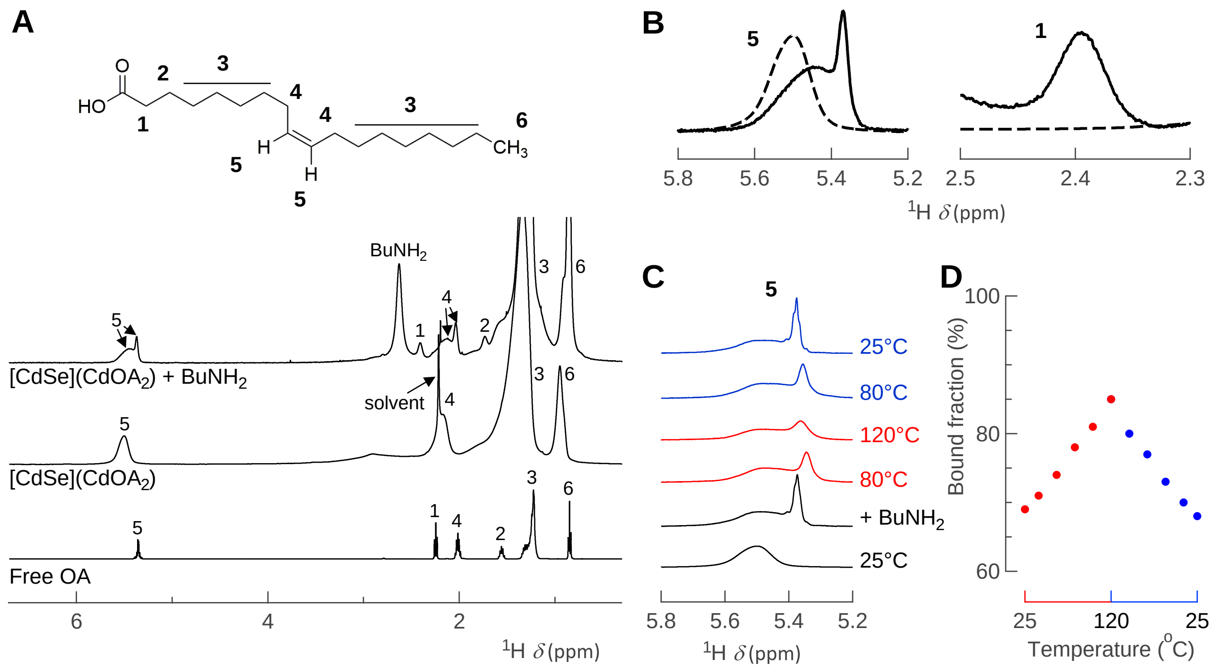

Figure 2: (a) ^{1}H NMR spectrum of (bottom) oleic acid (OA) dissolved in 1,2-dichlorobenzene-d_4 (DCB), (middle) a dispersion of 3.4 nm [CdSe]($CdOA_2$) NCs in DCB, with an estimated NC concentration of 225.1 μM and a bound OA concentration of 32.5 mM, and (top) the same sample after addition of 5 equiv of $BuNH_2$. (b) Zoom on the alkene resonance **5** and the $\alpha - CH_2$ resonances **1** of $CdOA_2$ (dashed lines) before and (full lines) after addition of 5 equiv of $BuNH_2$ [same sample as in (a)]. (c) Overview of alkene resonance of the $CdOA_2$ capped CdSe NCs during an experiment where 3 equiv of $BuNH_2$ was added, followed by a temperature sweep from room temperature to 120℃ and back. (d) Bound fraction obtained by deconvolution of the alkene resonances during this temperature sweep from (red) 25℃ to 120℃ and (blue) back to 25℃.

appears as a distinct resonance at around 2.40 ppm upon addition of $BuNH_2$. These changes resemble [CdSe]($CdOA_2$) spectra recorded on dispersions to which an excess of oleic acid was added.[26] Similar to these systems, the broad resonances feature the small diffusion coefficient typical of bound ligands, whereas the new resonances have a diffusion coefficient close to that of free oleic acid (see Supporting Information, Section S2). In addition, we found that upon increasing the $BuNH_2$ concentration, the new, more narrow resonances gain intensity at the expense of the originally present broad resonances such that their joint intensity remains constant. We therefore assigned the additional upfield resonances to displaced oleate, which is most likely present as a $BuNH_2$-cadmium oleate complex.[13]

Figure 2c shows the alkene resonance recorded on a dispersion of [CdSe]($CdOA_2$) NCs to which 3 equiv of $BuNH_2$ – relative to $CdOA_2$ – was added, followed by a temperature sweep from room temperature to 120℃ and back. By deconvolution of the alkene resonance, the amounts of bound and displaced $CdOA_2$ can be derived from such spectra at different temperatures. Figure 2d indicates that the resulting fraction of displaced $CdOA_2$ drops upon increasing temperature and increases again when lowering the temperature, such that the same ratio is obtained for a given temperature during the forward and the backward sweep. This points towards a reversible dynamic equilibrium between bound and displaced OA and suggests an overall exothermic displacement reaction. De Roo *et al.* previously described an exothermic process when exchanging oleic acid for octylamine on HfO_2 NCs.[42] Importantly, a reference measurement in which a [CdSe]($CdOA_2$) dispersion without $BuNH_2$ is exposed to the same heating and cooling cycle shows that bound OA exhibits little self-desorption (see Supporting Information, Section S2). Hence, the concentration of bound and displaced OA, that follow from the resonance intensities in the NMR spectra, mostly reflect the effect of L-type promoted Z-type displacement, allowing us to analyze stoichiometry and thermodynamics of this reaction. As shown in the Supporting Information (Section S2), addition of benzylamine ($BnNH_2$) or tetramethylethylenediamine (TMEDA) leads to qualitatively similar changes in the ^{1}H NMR spectra. Also in these cases, we interpret the changes as reflecting the displacement of $CdOA_2$ by either of these L-type ligands and we will use the intensity of the different resonances to quantify the displacement equilibrium.

The Displacement Equilibrium

Figure 3a shows three displacement isotherms obtained on dispersions of 3.4 nm CdSe NCs at 60 ℃ after addition of $BnNH_2$, $BuNH_2$ and TMEDA, respectively. These isotherms represent the surface coverage θ of bound $CdOA_2$, *i.e.*, the remaining fraction of the original surface concentration of bound $CdOA_2$, as a function of the concentration of the L-type displacer added to the dispersion. The way we decomposed the NMR spectra into a bound and a displaced $CdOA_2$ contribution is outlined in more detail in section S3 of the Supporting Information. Focusing first on the isotherms of $BnNH_2$-induced $CdOA_2$ displacement, one sees that less then 0.1 mol/L (7 equiv in this case) of $BnNH_2$ suffice to displace a quarter of the originally bound $CdOA_2$, whereas more than 0.5 mol/L (35 equiv in this case) is needed to raise the displaced fraction above 0.5. Interestingly, addition of either $BuNH_2$ or TMEDA yields different isotherms with, in general, a more pronounced stripping. Moreover, it seems that TMEDA is the more effective displacer at low concentration, whereas $BuNH_2$ results in comparable displacement at higher concentrations. On the other hand, similar to $BnNH_2$-induced displacement, both isotherms exhibit a pronounced drop in surface coverage of $CdOA_2$ at low displacer concentration in combination with a persistent fraction of $CdOA_2$ at high displacer concentration.

Differences in displacement potency of various L-type ligands were already discussed by Anderson *et al.* and interpreted in terms of electronic effects, chelation and steric hindrance.[13] Starting from displacement isotherms, however, a more quantitative analysis of different displacing agents is possible in terms of the stoichiometry and the energetics of the displacement reaction. To do so, we write the displacement as a reaction driven by the coordination of surface bound $CdOA_2$ moieties by amines:

$$[\mathrm{CdSe}](\mathrm{CdOA_2}) + n\mathrm{L} \rightleftharpoons [\mathrm{CdSe}](\circ) + \mathrm{Cd(OA)_2L_n} \tag{1}$$

Here, L is a generic representation of an L-type ligand – $BnNH_2$, $BuNH_2$, or TMEDA in this case – and ($\circ$) represents an empty binding site for $CdOA_2$ at the CdSe surface. Based on the displacement equilibrium (Eq 1), an equilibrium expression can be written down that links the concentration of free amine and displaced $CdOA_2$ to the fraction of bound $CdOA_2$:

$$\frac{[\mathrm{Cd(OA)_2L_n}] \times (1-\theta)}{[\mathrm{L}]^n \times \theta} = K \tag{2}$$

Here, we have set the activity of dissolved species equal to their concentration and we have assumed that the activity of adsorbed species and free adsorption sites corresponds to their respective fractional occupation θ and $1-\theta$ of all available surface sites.

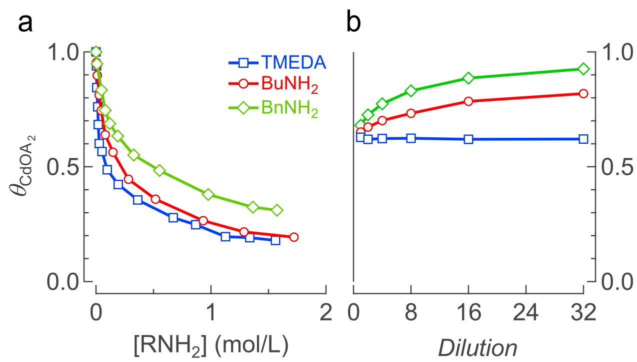

Figure 3: Experimental isotherms realized at 60℃ of the Z-type displacement reaction with $BnNH_2$ (green), $BuNH_2$ (red) and TMEDA (blue) on the $CdOA_2$ capped CdSe NCs. (B) Bound fraction of the $CdOA_2$ ligand in function of the dilution series (×1, ×2, ×4, ×8, ×16, and ×32) for all three displacers studied here. The error on the surface coverage varies from point to point, but is estimated on average at 5% (see Supporting Information, section S3).

Equation 2 can only be used to analyze experimental adsorption isotherms if the stoichiometry of the displacement reaction, *i.e.*, the number n of amine ligands coordinating a single displaced $CdOA_2$, is known. We therefore analyzed the shift of the displacement equilibrium with increasing dilution of the dispersion. As shown in the Supporting Information **Emile – Make sure the order of the SI is in line with the order it appears in the text. Not the case here.**, the ^{1}NMR spectrum of the alkene resonance – rescaled to the peak intensity of the displaced $CdOA_2$-resonance – hardly changes upon diluting the NC dispersion in the case that TMEDA is the displacer. This conclusion also follows from a more quantitative analysis of the ^{1}NMR spectra shown in Figure 3b, where in the case of TMEDA the fraction of bound oleate is indeed dilution-independent. Looking at Eqs 1 and 2, this is only possible when the number of dissolved species is the same at both sides of the reaction. Hence, we conclude that $n = 1$ in the case of TMEDA displacement, which confirms the idea already expressed by Anderson *et al.* that TMEDA acts as a chelating agent. On the other hand, when using $BnNH_2$ or $BuNH_2$ as the displacer, we found that dilution leads to a relative increase of the bound $CdOA_2$-resonance (see Figure S5b and Figure S5c respectively, in Supporting Information, Section S2 **Same remark on order of Figures in Supporting Info**), which translates into an increase in the fraction of surface-bound $CdOA_2$ as shown in Figure 3e. This shift towards adsorption upon dilution indicates that more dissolved species are present at the reagent side in the displacement equilibrium, *i.e.* $n > 1$, when $BnNH_2$ or $BuNH_2$ are used as a displacer. Since a single diamine such as TMEDA coordinates to a single $CdOA_2$, we tentatively take $n = 2$ for the case of mono-amines such as $BnNH_2$ or $BuNH_2$. We will come back to this assumption later.

When describing the displacement reaction using the chemical equilibrium expressed by Eqs 1 and 2, we discarded a possible coupling between the displacement of $CdOA_2$ by amines and the binding of amines to empty surface sites. We take this approach since alkylamines were found to bind only weakly to CdSe NCs, resulting in a dynamic adsorption/desorption equilibrium that requires a considerable excess of alkylamines to keep CdSe NC dispersions stable.[43] If binding of amines were an important part of the equilibrium, dilution would lead to amine desorption, and the concomitant increase of free adsorption sites would shift the equilibrium of Eq 1 to the left, i.e., to more bound $CdOA_2$. Hence, the fact that the TMEDA equilibrium is dilution insensitive confirms that in this case, amine adsorption/desorption is not an important side-reaction. Since the poor adsorption of TMEDA may be due to steric effects, we also analyzed the dilution-dependent displacement equilibrium upon addition of ethylenediamine (EDA), a diamine that has two primary amine functionalities unlike TMEDA. In this case, we found that dilution results in a slight shift of the displacement equilibrium towards more bound $CdOA_2$; a shift that is, however, considerably smaller than in the case of $BnNH_2$ and $BuNH_2$. Since EDA will be the stronger adsorbent, this suggests that the dilution-dependence of the displacement equilibrium in the case of $BnNH_2$ and $BuNH_2$ mainly reflects the 2 equiv displacement of $CdOA_2$.

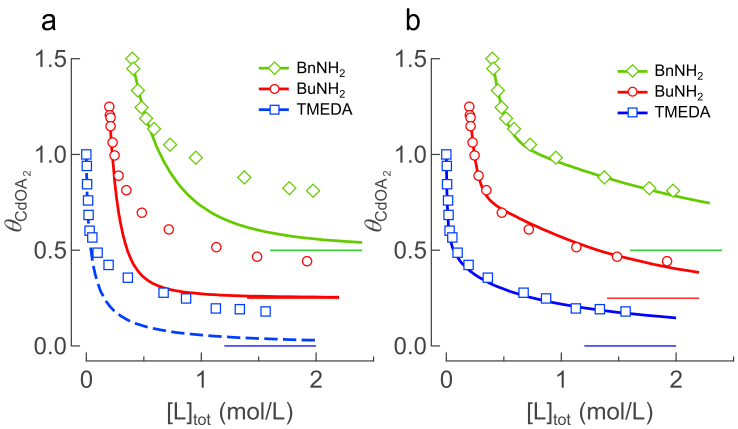

Figure 4: (A and B) Experimental isotherm points of $BnNH_2$, $BuNH_2$ and TMEDA (green, red and blue respectively). In (A), the respective expressions (n=1 for TMEDA and n=2 for $BnNH_2$ and $BuNH_2$) are used to fit the initial points of the isotherms assuming that all binding sites on the CdSe NCs are identical. And (B), The same, where the experimental isotherms are simulated using the two-site model assuming distinct binding sites.

Thermodynamic Analysis of Displacement Isotherms, the Two Site Model

The equilibrium expression (Eq 2) can be rewritten as a relation between θ and the total concentration of the displacer (see Supporting Information, Section S4). In Figure 4a, we used the respective expressions that apply when $n = 1$ or $n = 2$ to extrapolate the initial part of the isotherm in the case of all three amines used. For each experimental isotherm, we find that simulations forced to match the rapid initial drop of θ fail to account for the persistent presence of bound $CdOA_2$ at higher amine concentrations. As for the extrapolated simulations, the pronounced initial displacement of $CdOA_2$ should lead to full ligand displacement within the range of amine concentrations used. In reality, however, reducing the bound $CdOA_2$ fraction below ~ 0.5 is more difficult and requires far higher amine concentrations than expected based on the initial displacement at lower amine concentration.

Importantly, at $\theta = 0.5$, the ligand surface concentration remains well above the $\sim 0.3\,\mathrm{nm}^{-2}$ that was reported for carboxylic acid impurities in CdSe NC ligand shells and which would lead to tightly bound ammonium-carboxylate ion pairs.[43] Hence, it seems unlikely that this persistent binding of $CdOA_2$ is due to oleate moieties with a different binding motif.

When writing the displacement equilibrium using Eq 2, we assumed that the binding of $CdOA_2$ to CdSe NCs can be described by a single equilibrium constant K. This assumption is based on the conjecture that all binding sites are identical. Given the atomic structure of the NC surface, where surface atoms can be part of facets, facet edges or vertex sites at which 3 facets come together, surface sites may well differ in terms of the binding free energy for $CdOA_2$ moieties. As a result, a description of the surface in terms of a distribution of binding enthalpies may be more appropriate. In such a case, the displacement isotherm at low displacer concentration could be determined by loosely bound $CdOA_2$ moieties, while a fraction of more strongly bound $CdOA_2$ moieties would then explain the deviation between the experimental data and the extrapolated model isotherm. Clearly, this would require a variation of the binding free energy that is significant as compared to thermal energy.

Building on the idea of a distribution of binding energies, we adapted the analysis of the experimental isotherms using a two-site model, where surface $CdOA_2$ is either found on weaker or stronger binding sites, labeled here 1 and 2, respectively:

$$[\mathrm{CdSe}](\mathrm{CdOA_2})_1 + n\mathrm{L} \rightleftharpoons [\mathrm{CdSe}](\circ)_1 + \mathrm{Cd(OA)_2L_n} \tag{3}$$

$$[\mathrm{CdSe}](\mathrm{CdOA_2})_2 + n\mathrm{L} \rightleftharpoons [\mathrm{CdSe}](\circ)_2 + \mathrm{Cd(OA)_2L_n} \tag{4}$$

This coupled equilibrium translates into a set of two coupled nonlinear equations from which the total fraction of bound $CdOA_2$ can be calculated (see Supporting Information, Section

Table 1: Experimental data and model parameters used to described the displacement isotherms using a two-site adsorption model

Displacer	$CdOA_2$ (mol/L)	K_1	K_2	α
$BnNH_2$	0.017	0.8	0.004	0.5
$BuNH_2$	0.018	3.0	0.01	0.525
TMEDA	0.019	1.5	0.02	0.475

S4):

$$\frac{[\mathrm{Cd(OA)_2L_n}] \times (1-\theta_1)}{[\mathrm{L}]^n \times \theta_1} = K_1 \tag{5}$$

$$\frac{[\mathrm{Cd(OA)_2L_n}] \times (1-\theta_2)}{[\mathrm{L}]^n \times \theta_2} = K_2 \tag{6}$$

Here, we have used an approach similar to the one used in Eq 2 to express the activities of all species involved in both equilibria, where the indexes 1 and 2 refer to the two distinct adsorption sites.

To simulate the experimental isotherm using Eqs 5 and 6, we considered the respective equilibrium constants K_1 and K_2, and the fraction α of the weaker surface sites to be adjustable parameters. Figure 4b represents simulations of the experimental isotherms obtained for $BnNH_2$, $BuNH_2$ and TMEDA using the parameter set as given in Table 1. It can be seen that a two site model with distinct adsorption free energies captures the more difficult displacement of bound $CdOA_2$ at higher displacer concentrations, both in the case of a 1-equivalent (TMEDA) and a 2-equivalent displacement reaction ($BuNH_2$ and $BnNH_2$). Depending on the experiment, the fraction α of weakly binding sites can be slightly larger or somewhat smaller than 0.5, which suggests that at the start of the titration series, bound ligands are about equally spread over both binding sites.

Looking at the different parameter sets in Table 1, one sees that the ratio of K_1 and K_2 does vary, yet remains within the range $75 - 300$. This is important, since the reaction free energy of the displacement equilibria expressed by Eqs 3 and 4 only differs by the adsorption free energy of both sites, irrespective of the actual displacer used. Hence, while K_1 and K_2 can be different, the fact that their ratio is comparable shows that a 2-site model can give a reasonably consistent description of the displacement isotherms, irrespective of the actual displacer used. Note that a factor of 75-300 amounts to a reaction free energy difference of $12 - 16\,\mathrm{kJ/mol}$.

Comparing the parameters obtained for $BnNH_2$ and $BuNH_2$ – which were both described as 2 equiv displacers – we find that the more pronounced displacement induced by $BuNH_2$ translates into larger equilibrium constants. The corresponding difference in displacement free energy is, however, only $\sim 3.5\,\mathrm{kJ/mol}$. Moreover, the different equivalence of the displacement equilibrium for TMEDA ($n = 1$) and $BuNH_2$ ($n = 2$) explains why TMEDA is a more effective displacer at low concentration, while $BuNH_2$ can become a comparable displacer at high concentration. The fact that the equilibrium constants are about equal concurs with the experimental finding that both isotherms coincide for displacer concentrations of $\sim 1\,\mathrm{mol/L}$. Finally, as shown in the Supporting Information Section S5, the two-site model and the parameters used to simulate the displacement isotherms in the case of $BnNH_2$ and $BuNH_2$ can account for the dilution-induced readsorption of $CdOA_2$, which confirms the assumption that $n = 2$ in the case of displacement by primary amines.

Binding Site Heterogeneity, a Computational Confirmation

To support the conclusion that the surface of CdSe NCs offers a distribution of binding energies for $CdOA_2$ complexes, we performed density functional theory (DFT) calculations on a non-stoichiometric $\sim 3\,\mathrm{nm}$ CdSe NC with chemical formula $[CdSe]_{309}(CdCl_2)_{51}$. In this case, the excess of positive charge is neutralized with X-type chlorine ligands instead of carboxylates. We opted for this passivating ligand rather than a more suitable acetate ligand, because Cl offers a significant computational advantage and a less complicated exploration of the potential energy surface of the binding sites. As illustrated in Figure 5a, the model nanocrystal exposes three Cd-terminated and three Se-terminated (111) facets, and six stoi-

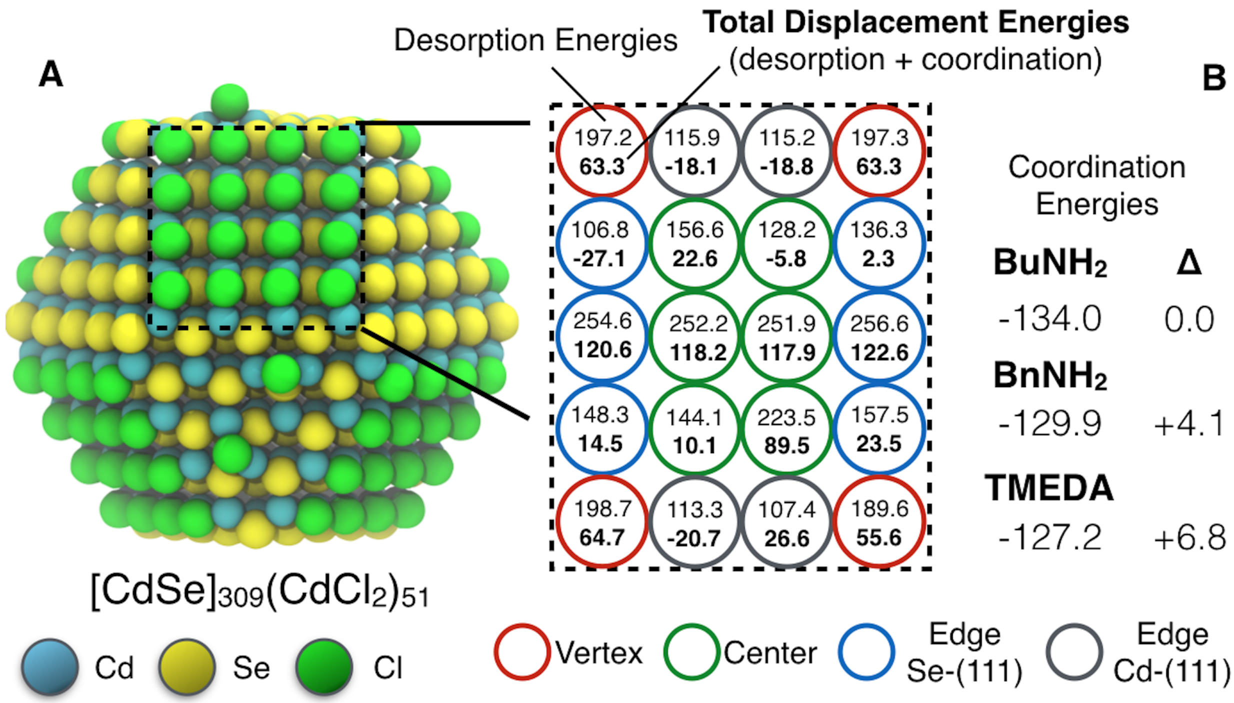

Figure 5: (A) Relaxed structure of the CdSe model ($\sim 3\,$nm) computed with the DFT/PBE level of theory. (B) Computed total displacement (desorption and coordination) energies, in kJ/mol, between the $CdCl_2$ ligand and the surface according to the chemical formula in (1) when utilizing $BuNH_2$ as the displacer. The coordination energies of $BuNH_2$, $BnNH_2$ and TMEDA is also indicated in kJ/mol.

chiometric (100) facets that are fully covered with Z-type $CdCl_2$ ligands. On this structure, we analyzed the energetics of the displacement of a $CdCl_2$ moiety induced by amines as outlined in the Experimental Section, reproducing in this way the chemical reaction expressed by Eq 1. We systematically displaced a $CdCl_2$ unit from a different binding site and fully relaxed the structure of the nanocrystal to account for geometrical reorganizations and determined the displacement (electronic) energy from the energy difference between the initial model nanocrystal and the fully relaxed final state, which includes the 1 equiv (TMEDA) or 2 equiv ($BuNH_2$, $BnNH_2$) coordination of the $CdCl_2$ unit by the displacer.

Figure 5b represents the desorption energies and the total displacement energies – the latter including the contribution from the coordination – as obtained when using $BuNH_2$ as the displacer. Similar displacement energies are obtained for $BnNH_2$ and TMEDA, the only difference coming from slightly weaker coordination energies. Figure 5b shows that

$CdCl_2$ desorption energies strongly vary across a CdSe (100) facets, spanning a wide range from 106.8 to 256.6 kJ/mol. Moreover, 2 equiv coordination with $BuNH_2$ leads to slightly exothermic displacement energies for the weaker adsorption sites. Inspection of the relaxed nanocrystal structures obtained after $CdCl_2$ displacement, enabled us to identify a few trends. Removal from the edge positions with the Cd-rich (111) facets is the most favourable, and is slightly exothermic; a similar trend is found for the displacement from the edge positions with the Se-rich (111) facets, however in this case the displacement is slightly endothermic and from the central (edge) position is highly disfavoured; displacement from the vertex positions is rather endothermic and in all cases, surface reconstruction leads to the formation of di-coordinated Se atoms, which have been proposed as a source of surface traps.[14]

Overall, we find that 11 out of 20 adsorption sites have binding energies slightly above or slightly below 0 kJ/mol – an average of -3 kJ/mol is obtained for $BuNH_2$ – whereas the remaining 9 binding sites are strongly endothermic. Note that this distinction also applies to pure (100) positions, where we could discern three weaker and three stronger binding sites. Inspection of the relaxed structures shows that from these latter sites, Cd ions migrate from the central position to the edge position providing more favorable displacement energetics. Taken all this findings together, we conclude that DFT calculations confirm that adsorption sites are present with widely varying adsorption energies, depending on the position of the binding site on the nanocrystal facet. Moreover, the counteracting effect of endothermic desorption and exothermic coordination is such that slight variations of the coordination energy can result in either endothermic or exothermic net displacement energies.

Thermodynamic Displacement Descriptors, Experiment and Theory

To have a more direct comparison between the experimental isotherms and the binding energies calculated by DFT, we analyzed in more detail the temperature dependence of the ligand surface coverage. As shown in Figures 6a-c, a temperature increase reverses ligand

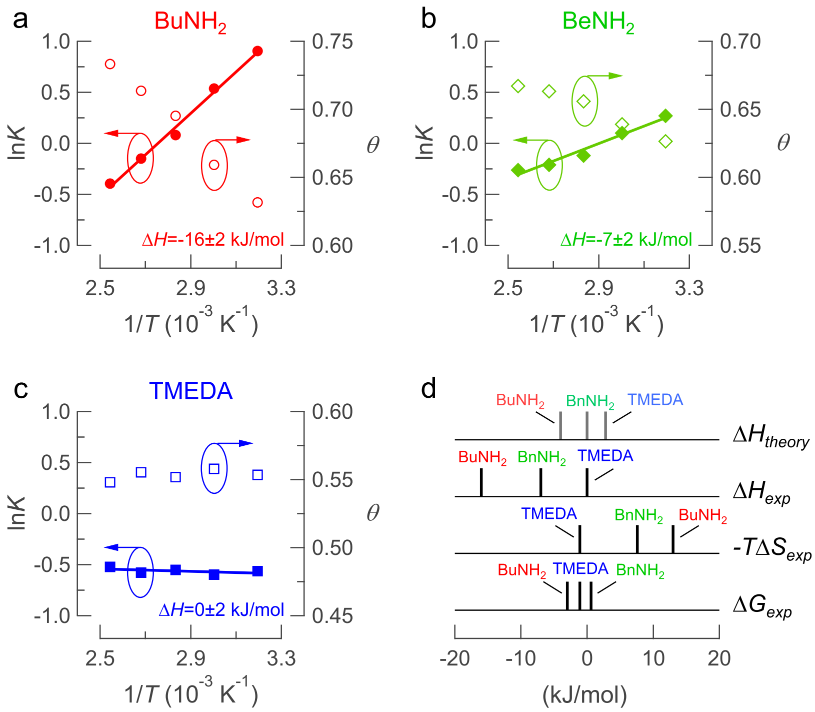

Figure 6: (a-c) Representation of (open symbols) fractional occupation and (closed symbols) logarithm of the equilibrium constant K_1 for (red) $BuNH_2$ displacement, (green) $BnNH_2$ displacement, and (blue) TMEDA displacement as a function of the inverse temperature. The full line represents a best linear fit through the data. (d) Representation of the (top) average displacement enthalpy calculated using DFT for the fraction of weaker binding sites, (second from top) displacement enthalpy as estimated from the van 't Hoff plots shown in (a-c), (third from top) entropy contribution $T\Delta S$ to the reaction free energy and (bottom) reaction free energy at 60°Cas obtained from the equilibrium constants K_1 as listed in Table 1. The entropy contribution is calculated so as to match the difference between the displacement free energy and the displacement enthalpy.

displacement in the case of both $BuNH_2$ and $BnNH_2$, whereas the displacement equilibrium is largely temperature independent in the case of TMEDA. Assuming that the strongly binding adsorption sites are still fully occupied under the conditions of the temperature sweep, the reaction enthalpy for the desorption of the more loosely bound ligands can be estimated from the variation of the displacement equilibrium with temperature (see Supporting Information Section S6). The resulting variation of $\ln K_1$ with temperature are included as van 't Hoff plots in Figures 6a-c, from which we get a ΔH_1 varying from -16 ± 2 kJ/mol for $BuNH_2$ to -7 ± 2 kJ/mol for $BnNH_2$, and to 0 ± 2 kJ/mol for TMEDA. These borderline exothermic/endothermic displacement enthalpies indicate that the sites initially affected by the displacer correspond to the weaker binding sites identified from DFT. In line with the experiment, these weaker binding sites correspond to around 50% of all sites. Moreover, as shown in Figure 6d, experiment and theory also agree on the relative order of ΔH_1, yielding $BuNH_2$ as the most exothermic displacer and TMEDA as the most endothermic one. Note that this correspondence strongly depends on the coordination; if we were to describe $BuNH_2$ or $BnNH_2$ as 1 equiv displacers, DFT simulations would yield strongly endothermic displacement energies and they would be far weaker displacers than TMEDA.

An intriguing element of the displacement equilibrium is that while TMEDA is the weakest displacer in terms of reaction enthalpy, its equilibrium constant K_1 is in between that of $BuNH_2$ and $BnNH_2$ and it effectively displaces most $Cd(OA)_2$ at low displacer concentrations. We already interpreted the latter point in terms of chelation by TMEDA, where a single TMEDA suffices to complex a single $Cd(OA)_2$. Chelation, however, not only changes the reaction quotient, it also influence the equilibrium constant K_1. Combining the displacement free energies as calculated from the estimated equilibrium constants (see Table 1) and the reaction enthalpies, the entropy contribution to the standard reaction free energy can be estimated. As shown in Figure 6, TMEDA stands out in this respect as it has an entropy contribution $T\Delta S$ to the reaction free energy that is 9 to 14 kJ/mol more favorable than in the case of $BnNH_2$ and $BuNH_2$, respectively. This is closely in line with the different stoichiometry of the displacement reaction. Indeed, each dissolved species at the reagent side increases the standard reaction free energy by $-RT\ln(V_m c_0)$, where V_m is the molar volume of the solvent and c_0 the standard concentration; a term related to entropy of mixing. Hence, using the molar volume of 1,2-dichlorobenzene, an entropy contribution more positive by $-RT\ln(V_m c_0) = 6.0$ kJ/mol is expected for 2 equiv displacers such as $BnNH_2$ and $BuNH_2$. This difference – which only counts effects of entropy of mixing – is in reasonable agreement with the estimated changes of $T\Delta S$ for the different displacers as plotted in Figure 6. We thus conclude that equilibrium constants as summarized in Table 1 result from subtle trade-offs at the level of displacement enthalpy and displacement entropy, especially when 1 equivalent and 2 equivalent displacers are concerned.

Quantitatively, the difference between K_1 and K_2 seems small as compared to the $50-100\,\mathrm{kJ/mol}$ difference in binding energy for the weaker and stronger binding sites estimated from DFT. Possibly, this is related to the calculations performed in vacuum at 0K or to the arbitrary choice of the displaced $CdCl_2$ fragment, where the chlorine atoms bound to cadmium can be selected from different positions. In addition, the experimental displacement reaction starts with [CdSe]($CdOA_2$) NCs that have an OA surface concentration of $4.0\,\mathrm{nm}^{-2}$ that drops at the highest displacer concentrations to $\sim 0.7\,\mathrm{nm}^{-2}$. Hence, the experiment may not probe the strongest binding sites as calculated for the model nanocrystal. Moreover, during the experiment, the surface concentration of ligands progressively drops, whereas the simulations always start from a fully terminated surface to calculate site-dependent adsorption energies. In this respect, one should note that surface reconstruction and the concomitant relaxation energies, which are included in the calculations, can be affected by the overall ligand surface concentration and may be hampered in reality by kinetic barriers.

Discussion

Even if is difficult to link the full distribution of the computational binding energies to the data provided by the two-site model, both results indicate that a description of colloidal CdSe nanocrystals as objects offering one specific binding site for CdX_2 complexes is too much of a simplification. Rather, the surface hosts a variety of binding sites, which feature a wide distribution of binding energies depending on the actual position of the site on the nanocrystal surface. This results in displacement isotherms that combine a pronounced loss of ligands at low displacer concentration with a fraction of bound ligands that persists even at high displacer concentrations. Moreover, in the case of the weaker binding sites, the desorption and coordination energies almost match. Depending on the actual displacer used, this results in slightly exothermic displacement reactions, for which an increase in temperature drives displaced CdX_2 back to the surface.

From a more general perspective, this binding site heterogeneity implies that the effect of any ligand exchange reaction can strongly depend on the initial surface concentration of ligands. Consider, for example, two batches of similar nanocrystals where one has a higher surface concentration of ligands than the other. In such a case, mostly strongly bound ligands will remain on the low surface concentration nanocrystals, whereas plenty of loosely bound ligands can still be present on the high surface concentration nanocrystals. For one thing, this makes that the isotherms used here to quantify displacement reactions will not be uniquely defined. This is illustrated in the Supporting Information Section S7, where two $BuNH_2$ isotherms are shown that have been obtained using two batches of CdSe nanocrystals with a different initial surface concentration. One sees that the isotherms have a different shape, where in particular the initial displacement is less pronounced in the case of the QDs with the lower initial surface concentration. This makes that this isotherm requires a smaller equilibrium constant for the weak binding sites and a lower fraction of weakly bound ligands to be simulated using the two-site model, a finding in line with the idea that ligands preferably occupy binding sites with a higher binding energy.

Conclusion

We used solution NMR to quantify the displacement of Z-type $CdOA_2$ ligands from CdSe QDs by addition of L-type ligands. We addressed the stoichiometry of the displacement reaction by analyzing the shift of the dynamic equilibrium upon dilution and the displacement thermodynamics were studied by analyzing displacement isotherms. We found that using a diamine such as TMEDA as the displacer results in a 1 equivalent displacement reaction, whereas 2 equivalents of a primary amine such as $BuNH_2$ or $BnNH_2$ bind to 1 equivalent of displaced $CdOA_2$. Regardless of the displacer used, we showed that the displacement isotherms cannot be described using a single chemical equilibrium reaction, in which the CdSe surface is described as a substrate offering a set of identical adsorption sites for $CdOA_2$. On the other hand, a consistent description of the experimental isotherms was possible by means of a more complex model, which included two types of binding sets with a different binding energy. The assumption of binding site heterogeneity that underlies this approach was further confirmed by DFT calculations on a CdSe model QD, which showed that a single (100) facet indeed contains a distribution of binding sites with a widely varying adsorption energy. Since ligands preferably bind to sites offering the highest binding energy, this implies that nanocrystal surface treatments can be faced with a population of strongly bound ligands that are difficult to displace or exchange and it makes that the effect of such treatments can depend on the initial surface concentration of ligands. Moreover, since this distribution of binding energy results from the presence of a large fraction of edge and vertex sites on the nanocrystal facets, this finding is most likely not restricted to CdSe NCs, and should be considered when analyzing surface reactions on any nanocrystal.

Acknowledgement

The authors acknowledge the European Commission via the Marie Sklodowska-Curie Action Phonsi (H2020-MSCA-ITN-642656), BelSPo (IAP 7.35, photonics@be), FWO-Vlaanderen (KaN 1509012N), Ghent University (GOA/01G01513; BOF14/PDO/007), and IWT-Vlaanderen for financial support. The 500 MHz equipment used in this work was funded through a grant from the Hercules foundation (AUGE09/006). I. I. would like to thank the Netherlands Organization of Scientific Research (NWO) for providing financial support within the Innovational Research Incentive (Vidi) Scheme (Grant No. 723.013.002). This work was carried out on the Dutch national e-infrastructure with the support of SURF Cooperative.

Supporting Information Available

This material is available free of charge via the Internet at `http://pubs.acs.org/`.

References

(1) Boles, M. A.; Ling, D.; Hyeon, T.; Talapin, D. V. *Nat. Mater.* **2016**, *15*, 141–153.

(2) De Roo, J.; De Keukeleere, K.; Hens, Z.; Van Driessche, I. *Dalton Trans.* **2016**, *45*, 13277–83.

(3) Yin, Y.; Alivisatos, A. P. *Nature* **2005**, *437*, 664–70.

(4) Wang, F.; Buhro, W. E. *Journal of the American Chemical Society* **2012**, *134*, 5369–5380.

(5) Reiss, P.; Carriere, M.; Lincheneau, C.; Vaure, L.; Tamang, S. *Chem. Rev.* **2016**, *116*, 10731–819.

(6) Gerdes, F.; Navio, C.; Juarez, B. H.; Klinke, C. *Nano Lett.* **2017**, *17*, 4165–4171.

(7) Lee, J.; Sundar, V. C.; Heine, J. R.; Bawendi, M. G.; Jensen, K. F. *Adv. Mater.* **2000**, *12*, 1102–1105.

(8) Pellegrino, T.; Manna, L.; Kudera, S.; Liedl, T.; Koktysh, D.; Rogach, A. L.; Keller, S.; Rdler, J.; Natile, G.; Parak, W. J. *Nano Lett.* **2004**, *4*, 703–707.

(9) Frederick, M. T.; Weiss, E. A. *ACS Nano* **2010**, *4*, 3195–200.

(10) Brown, P. R.; Kim, D.; Lunt, R. R.; Zhao, N.; Bawendi, M. G.; Grossman, J. C.; Bulovic, V. *ACS Nano* **2014**, *8*, 5863–72.

(11) Owen, J. *Science* **2015**, *347*, 615–6.

(12) Giansante, C.; Infante, I.; Fabiano, E.; Grisorio, R.; Suranna, G. P.; Gigli, G. *J. Am. Chem. Soc.* **2015**, *137*, 1875–86.

(13) Anderson, N. C.; Hendricks, M. P.; Choi, J. J.; Owen, J. S. *J. Am. Chem. Soc.* **2013**, *135*, 18536–18548.

(14) Houtepen, A. J.; Hens, Z.; Owen, J. S.; Infante, I. *Chem. Mater.* **2017**, *29*, 752–761.

(15) Talapin, D. V.; Lee, J. S.; Kovalenko, M. V.; Shevchenko, E. V. *Chem. Rev.* **2010**, *110*, 389–458.

(16) Chuang, C.-H. M.; Brown, P. R.; Bulovi, V.; Bawendi, M. G. *Nature materials* **2014**, *13*, 796–801.

(17) Lan, X.; Voznyy, O.; Garcia de Arquer, F. P.; Liu, M.; Xu, J.; Proppe, A. H.; Walters, G.; Fan, F.; Tan, H.; Liu, M.; Yang, Z.; Hoogland, S.; Sargent, E. H. *Nano Lett.* **2016**, *16*, 4630–4.

(18) Kovalenko, M. V.; Scheele, M.; Talapin, D. V. *Science* **2009**, *324*, 1417–20.

(19) Cros-Gagneux, A.; Delpech, F.; Nayral, C.; Cornejo, A.; Coppel, Y.; Chaudret, B. *J. Am. Chem. Soc.* **2010**, *132*, 18147–57.

(20) Norman, Z. M.; Anderson, N. C.; Owen, J. S. *ACS Nano* **2014**, *8*, 7513–21.

(21) De Roo, J.; Van Driessche, I.; Martins, J. C.; Hens, Z. *Nat. Mater.* **2016**, *15*, 517–21.

(22) Kroupa, D. M.; Voros, M.; Brawand, N. P.; McNichols, B. W.; Miller, E. M.; Gu, J.; Nozik, A. J.; Sellinger, A.; Galli, G.; Beard, M. C. *Nat. Commun.* **2017**, *8*, 15257.

(23) Wang, Y.; Fedin, I.; Zhang, H.; Talapin, D. V. *Science* **2017**, *357*, 385–388.

(24) Green, M. L. H. *J. Organomet. Chem.* **1995**, *500*, 127–148.

(25) Owen, J. S.; Park, J.; Trudeau, P. E.; Alivisatos, A. P. *J. Am. Chem. Soc.* **2008**, *130*, 12279–81.

(26) Fritzinger, B.; Capek, R. K.; Lambert, K.; Martins, J. C.; Hens, Z. *J. Am. Chem. Soc.* **2010**, *132*, 10195–201.

(27) Gomes, R.; Hassinen, A.; Szczygiel, A.; Zhao, Q.; Vantomme, A.; Martins, J. C.; Hens, Z. *J. Phys. Chem. Lett.* **2011**, *2*, 145–152.

(28) Zherebetskyy, D.; Scheele, M.; Zhang, Y.; Bronstein, N.; Thompson, C.; Britt, D.; Salmeron, M.; Alivisatos, P.; Wang, L. W. *Science* **2014**, *344*, 1380–4.

(29) Campos, M. P.; Owen, J. S. *Chem. Mater.* **2016**, *28*, 227–233.

(30) Walravens, W.; De Roo, J.; Drijvers, E.; Ten Brinck, S.; Solano, E.; Dendooven, J.; Detavernier, C.; Infante, I.; Hens, Z. *ACS Nano* **2016**, *10*, 6861–70.

(31) Sandeep, C. S.; Azpiroz, J. M.; Evers, W. H.; Boehme, S. C.; Moreels, I.; Kinge, S.; Siebbeles, L. D.; Infante, I.; Houtepen, A. J. *ACS Nano* **2014**, *8*, 11499–511.

(32) Whitham, K.; Yang, J.; Savitzky, B. H.; Kourkoutis, L. F.; Wise, F.; Hanrath, T. *Nat. Mater.* **2016**,

(33) Whitham, K.; Hanrath, T. *J. Phys. Chem. Lett.* **2017**, *8*, 2623–2628.

(34) Aruda, K. O.; Amin, V. A.; Thompson, C. M.; Lau, B.; Nepomnyashchii, A. B.; Weiss, E. A. *Langmuir* **2016**, *32*, 3354–64.

(35) De Nolf, K.; Cosseddu, S. M.; Jasieniak, J. J.; Drijvers, E.; Martins, J. C.; Infante, I.; Hens, Z. *J Am Chem Soc* **2017**, *139*, 3456–3464.

(36) Flamee, S.; Cirillo, M.; Abe, S.; De Nolf, K.; Gomes, R.; Aubert, T.; Hens, Z. *Chem. Mater.* **2013**, *25*, 2476–2483.

(37) Karel Capek, R.; Moreels, I.; Lambert, K.; De Muynck, D.; Zhao, Q.; Van Tomme, A.; Vanhaecke, F.; Hens, Z. *J. Phys. Chem. C* **2010**, *114*, 6371–6376.

(38) Parr, R. G.; Yang, W. *Density-Functional Theory of Atoms and Molecules*; Oxford University Press, 1989; p 333.

(39) Perdew, J. P.; Burke, K.; Ernzerhof, M. *Phys. Rev. Lett.* **1997**, *78*, 1396–1396.

(40) VandeVondele, J.; Hutter, J. *J. Chem. Phys.* **2007**, *127*, 114105.

(41) Hutter, J.; Iannuzzi, M.; Schiffmann, F.; VandeVondele, J. *Wiley Interdiscip. Rev. Comput. Mol. Sci.* **2014**, *4*, 15–25.

(42) De Roo, J.; Justo, Y.; De Keukeleere, K.; Van den Broeck, F.; Martins, J. C.; Van Driessche, I.; Hens, Z. *Angew. Chem. Int. Ed.* **2015**, *54*, 6488–91.

(43) Chen, P. E.; Anderson, N. C.; Norman, Z. M.; Owen, J. S. *J. Am. Chem. Soc.* **2017**, *139*, 3227–3236.

Graphical TOC Entry